NOTE: This document was excerpted from a larger report and is not citable.

This section of the *Illex illecebrosus* Research Track Stock Assessment will be presented to the MAFMC SSC by Lisa Hendrickson, Northeast Fisheries Science Center

TOR 3: Utilize the age, size and maturity dataset, collected from the 2019 landings, to identify the dominant intra-annual cohorts in the fishery and to estimate growth rates and maturity ogives for each cohort. Also use these data to identify fishery recruitment pulses.

Squid have a unique life history characterized by primarily sub-annual lifespans, semelparous reproduction with intra-annual cohorts, highly variable inter-annual abundance and rapid growth rates with high plasticity due to their close linkage with environmental conditions (Jackson and O'Dor 2001, Rodhouse *et al.* 2014, Doubleday *et al.* 2016). These traits make squid stocks difficult to assess and manage (Arkhipkin *et al.* 2020), especially transboundary ommastrephid stocks like *Illex illecebrosus* and *Illex argentinus*. Both stocks also have similar assessment and management challenges, for example, they both have extremely broad geographic ranges that extend across the regulatory jurisdictions of multiple Coastal States and a Regional Fisheries Management Organization (Figure 1.1) in the case of *I. illecebrosus* (Arkhipkin *et al*. 2015). *I. illecebrosus* and *I. argentinus* have such similar life histories that they both serve as a life history model for the *Illex* genus (Rodhouse *et al.* 1998).

Illex illecebrosus is a sub-annual, semelparous species for which ageing studies have shown that spawning occurs year-round with seasonal peaks that result in intra-annual cohorts (Dawe and Beck 1997, Hendrickson 2004). The latter study identified the winter cohort and determined that it supported the early portion of the U.S. *I. illecebrosus* fishery. Based on the average lifespan of the winter cohort, a second cohort (identified then as the spring cohort) was inferred and believed to support the latter part of the fishery period (Hendrickson 2004). The same study was the first to identify the spawning grounds and describe the age, growth and maturity of the southern stock component (i.e., the portion of the *I. illecebrosus* stock managed by the U.S.). The spawning grounds for the winter cohort is located in the Mid-Atlantic Bight near the edge of the continental shelf and within the U.S, fishing grounds where mature males and females have been caught in the directed fishery (Hendrickson 2004, Hendrickson and Hart 2006). This is the spawning grounds for the entire stock because mature and mated squid have never been captured in the Slope Sea and only a few mature females have been caught in colder Canadian waters (Hendrickson 2004). The 2019 and 2020 biological datasets described here were collected throughout the U.S. fishing season so they should be useful for confirming the winter cohort identification and identifying the second cohort and determining which months of the fishery that each cohort supports. In addition, the length, weight and maturity data from the 2019 fishery are also characterized.

Due to the time-consuming nature of processing and reading daily increments on cephalopod hard structures, there are few studies that have investigated population structure based on age analysis in this species (Morris and Aldrich 1984, Dawe *et al.* 1985, Dawe and Beck 1997, Hendrickson 2004). However, age rather than length data must be used to identify intra-annual cohorts and to estimate growth rates because squid growth rates show high plasticity, so individuals of the same mantle length can be from different intra-annual cohorts (Pierce and Guerra 1994, Arkhipkin *et al.*

2000, Arkhipkin *et al.* 2020). Without time-consuming population age studies to reveal the cohort structure, cohort assignment based on modal lengths may be misleading (Caddy 1991).

Cohort assignment itself is crucial for the sustainable management of squid stocks because differences in growth and maturation rates between cohorts require each cohort to be assessed separately as if it were a separate stock (Arkhipkin *et al.* 2020). A good reminder of the need for cohort-specific management of squid stocks is the collapse of the northern stock component (NAFO Subareas 3+4) of *I. illecebrosus* (Rodhouse *et al.* 1998) in 1982, following record high catches during 1976-1981 (Figure 1.2). The collapse subsequently led to a 36-year period of low productivity during 1982-2017 that could not support a fishery on this stock component (Hendrickson and Showell 2019).

Objectives of the 2019 and 2020 studies were to use statolith-based age analysis to identify the intra-annual cohorts that support the U.S. *I. illecebrosus* fishery and to summarize the biological data (i.e., DML, body weight and age) collected from the 2019 fishery samples. The 2020 study was conducted with grant funds awarded to Hendrickson after the Terms of Reference (TORs) for the *Illex* Research Track Assessment were established. This funding allowed a postdoctoral squid ageing and Trace Element Analysis (TEA) expert, Jessica Jones from the Falkland Islands, to conduct this research at the NEFSC. Thus, two additional objectives of the 2020 study were to improve the temporal resolution of the biological dataset through biweekly sampling of the fishery and to combine the age analysis with trace element analysis (TEA) of the statolith microstructure to determine whether the intra-annual cohorts have unique elemental signatures and to identify the ontogenetic migration patterns of the sampled individuals throughout their lifespans. However, for the reasons described below, only the former objective could be addressed in time for inclusion of the results in this report. For the same reasons, much of the biological data analyses focus on the age analyses.

BIOLOGICAL SAMPLING

Methods

Biological data were collected from unculled samples of *Illex* catches from the U.S. *Illex* fishery during 2019 and 2020. Each sample was collected from a known vessel, trip date and fishing location. The samples were provided by two *Illex* processors, Lunds Fisheries (Cape May, New Jersey) and The Town Dock (pack-out facility located in New Bedford, MA). Upon arrival at the processing plant, catches were randomly sampled, packed in boxes with trip identifier information, and then flash frozen. Samples were provided for June to October 2020, but May and September samples were not available due to COVID-19 pandemic-related issues. The samples were obtained from the catches of both fleet types, RSW boats and FT boats that did not cull their catches, were from trips conducted on both the northern and southern fishing grounds, in Southern New England and the Mid-Atlantic Bight regions, respectively (Figure 3.1). The frozen samples were later provided for two studies, referred to here as the 2019 and 2020 studies, although most of the dissection and ageing work occurred during 2020 and 2021, respectively.

The COVID-19 pandemic severely delayed analysis of the 2020 data because Jones was prevented from entering the U.S. when planned. This delayed Hendrickson's stock assessment analyses

because she had to conduct most of the biological data collection and statolith extractions. Closure of the London laboratory where the TEA equipment was located forced Jones to make alternative plans to accomplish this research. These delays prevented Jones from completing her TEA research as planned. However, she and Hendrickson will complete this research and publish it following the *I. illecebrosus* Management Track Assessment process. However, the results of analyses that could be completed in time, including a preliminary analysis of one of the trace elements, strontium, is presented.

Biological data for both years were collected in the laboratory from thawed specimens using the methods described in Hendrickson (2004). Dorsal mantle length (DML, mm), body weight (g), sex and sexual maturity stage were recorded for all specimens. Sex and maturity stage were assessed according to Mercer (1973) for males (stages 1-4) and Durward *et al.* (1979) for females (stages 1-5). Statoliths were extracted from all specimens and stored in 96% ethanol. For the 2019 samples, the MAFMC retained marine biologists from a consulting firm to collect the biological data following in-person training by Hendrickson and with her daily oversight. Age determinations were conducted by a European consultant with *Illex illecebrosus* ageing experience. Biological data collection and statolith extractions for the 2020 samples were conducted by Hendrickson and Jones. Age determinations were conducted by Jones, whose statolith-based squid ageing experience is extensive. Specimens subsampled for age analysis were representative of the sex ratios. The 2020 age subsamples were subsampled a second time to select individuals for TEA to ensure that biweekly samples, both sexes and a range of sexual maturity stages were represented.

Results

The *Illex* samples provided by the squid processors for biological data analysis are representative of the 2019 and 2020 directed fisheries (Figure 3.1). The samples are also temporally representative of the fisheries during both years, although sampling months differed between years due to different temporal sampling objectives and sample availability during the 2020 pandemic. During 2019 and 2020, the numbers of squid sampled for DML, body weight, sex and sexual maturity totaled 951 (during May-June and August-October) and 1,269 (during June-August and October), respectively (Table 3.1). The numbers of aged individuals for the same months (except for the 2019 October samples, which were not aged) totaled 400 in 2019 and 325 in 2020 (Table 3.1), which represent large sample sizes relative to many other statolith-based squid ageing studies.

AGEING

Methods

Squid ageing is extremely labor intensive and requires mounting, grinding and polishing both sides of the statolith prior to counting the daily growth increments. Daily increment periodicity has been validated in *I. illecebrosus* using two different chemical markers (Dawe *et al*. 1985, Hurley *et al*. 1985), therefore the total number of growth increments was considered to represent the post hatching age in days, with the nucleus (natal ring) representing the date of hatching (Balch *et al.* 1988).

For the 2019 samples, preparation of statoliths for increment counts involved mounting one statolith from each pair on a microscope slide with Crystalbond™ 509 mounting adhesive, with the anterior concave side uppermost. Statoliths were ground first on the anterior surface and then on the posterior surface. Grinding of both surfaces in the sagittal plane was done to produce relatively thin statolith sections that improved the visibility of growth increments. Increments were counted by eye along the axis of maximum statolith growth with a Nikon compound microscope at 400x magnification. In statoliths of the oldest individuals, when the increments were not clear enough to see (especially at the edge of the statolith or near the nucleus due to statolith crystallization), the number of unclear increments was estimated by extrapolation from the adjacent area. Observed age was the average of two sets of increment counts conducted on separate dates.

For the 2020 *Illex* age samples, one statolith per specimen was mounted for both elemental and age analysis, concave side up using Crystalbond™ 509 mounting adhesive (Aremco Products Inc.), then ground using wet waterproof silicon carbide grinding paper (P1200 followed by P2400 grit, Buehler) and polished (Buehler polishing cloth) on one side to expose the nucleus (Arkhipkin and Shcherbich 2012). Statoliths were then flipped and ground on the other side, embedded in mounting media (Canada Balsam™) and covered with a cover glass for observation (Arkhipkin and Perez 1998; Arkhipkin and Shcherbich 2012). Growth increments were counted manually, under the transmitted light of an Olympus BX60 compound microscope at 400x magnification. Increments were counted from the nucleus to the edge of the dorsal dome using an eyepiece reticle (Morris and Aldrich 1984; Arkhipkin and Laptikhovsky 1994; Arkhipkin *et al.,* 2000). Observed age was the average of two increment counts per statolith, conducted on separate dates.

Results

Linear regression models run on the two sets of statolith increment counts for each year were statistically significant ($p < 0.0001$) and explained model variance was high ($r^2 = 0.89$) and the same for both models. Residual standard errors were 6.9 and 7.9 for the 2019 and 2020 models, respectively. The residuals plot showed a slight bias in the age estimates of individuals older than 200 days, but the sample sizes for that age range were small for both years. Ages for 2019 and 2020 ranged between 107 and 221 days for 2019 and between 78 and 217 days for 2020. Although the maximum ages were similar, the minimum age for the 2020 data was about 30 days younger, mainly due to the smaller individuals from the summer cohort that recruited to the fishery in October (Table 3.2). The mean ages of males and females from the winter cohort were similar within each catch month during both years, with mean ages ranging between 147 and 178 days. However, females were larger than males, in both mantle length and body weight, as has been shown in other studies (Dawe and Beck 1997; Hendrickson 2004). The exception was June of 2020 when both males and females averaged 95 g and were only half the weight of the 2019 June samples. Recruitment of the summer cohort to the fishery primarily occurred during October, but a small portion also occurred in September of 2019. Mean ages for the summer cohort were about 104 days and 116 days, for females and males, respectively (Table 3.3). Mean DML and body weights for each sex were similar between the winter and summer cohorts.

Catch length and age compositions

Catch length and age compositions were computed for each year. Catch length frequencies were computed by multiplying the numbers-at-length pooled across all length subsamples by a length expansion factor. The length expansion factor was computed as the catch weight of *I. illecebrosus* pooled across all trips divided by the subsample weight of the length samples pooled across all trips. Catch length frequencies were then binned by 10-mm intervals. The same procedure was used to compute catch age frequencies for each year, but instead numbers-at-age pooled across all subsamples were expanded to the combined catch from all trips using the same length expansion factor. The hatch month frequency distributions for each year were computed as proportions of the pooled catch across all trips. To do so, catch numbers-at-length for all trips combined (computed as previously described) were multiplied by the proportions at length by hatch month.

Catch length and age compositions were unimodal for 2019 and bimodal for 2020 (Figure 3.2). The 2020 bimodalities were attributable to recruitment of the summer cohort to the fishery in October. Modal lengths and ages for 2020 occurred at 80 and 180 mm and 12 and 24 weeks. The 2019 modal length of the catch (210 mm) was slightly larger and the modal age was slightly younger (22 weeks).

Maturity

No juveniles were caught in the 2019 fishery samples. Modes of female maturity Stages 1, 2 and 3 (immature and maturing) occurred in the catches during May, June and September, respectively. Modes of male maturity Stages 1-3 (immature and maturing) occurred during May, June and August, respectively. The mode for mature males occurred during September. However, there were only 16 mature females in the samples, only six of which were aged. The low percentage of mature females was attributable to low sampling of the spawning grounds south of Hudson Canyon (Hendrickson 2004) during May and June.

INTRA-ANNUAL COHORT IDENTIFICATION

Methods

Intra-annual cohorts were identified from the 2019 and 2020 catch age frequency data pooled by hatch month. The age frequency distribution of each subsample was scaled up to the *I. illecebrosus* catch of the respective trip and binned by hatch month. The numbers-at-age in each trip subsample were multiplied by ratio of the trip catch weight of *I. illecebrosus* to the subsample weight of the aged specimens sampled from each trip. Trace element analysis (TEA) of the statolith microstructure, specifically the strontium sigantures of the winter versus summer cohorts, was used to confirm the cohort assignments that were based on the age frequency data by hatch month.

As reiterated in Arkhipkin *et al.* (2020), squid cohorts must be identified with age data because, due to high individual growth rate plasticity, squid of the same mantle length can be of different ages and from different intra-annual cohorts. Intra-annual cohorts that support the U.S. fishery, were identified from catch age frequency data that are shown as proportions of the age frequencies of the catch by hatch month. Ages were estimated from counts of statolith daily growth increments.

Results

As determined from a previous aging study (Hendrickson 2004), spawning occurs continuously during the U.S fishing season, so monthly fishery catches are comprisesd of a mix of individuals from two to four different hatch months (Figure 3.3). The results of the subject study confirmed the findings of Hendrickson (2004) that the winter cohort supports the early fishery period and a second cohort supports the remainder. The 2019 and 2020 age data allowed identification of the second cohort as the summer cohort, comprised of individuals hatched during May-July (Figure 3.4). September was a cohort transition month because the summer cohort recruited to the fishery in September of 2019, but most of the catch consisted of the winter cohort. The two datasets also showed that the winter cohort, comprised of individuals hatched during November-April, actually supported most of the fishery period, from May through September, which is a longer period than previously thought.

Proportions of the catch age frequency distribution differed by hatch month between the two years, in part, because of differential sampling between years; May-June and August-September (with no July or October samples) during 2019 and June-August and October (with no May or September samples) during 2020. For example, in 2019, the low proportions of individuals hatched in February and June and July were due to the lack of samples during July and October, respectively. Due to these temporal sampling differences, when the catch age frequency distributions of the two years are viewed together, it is clear that the modal hatch months of the winter and summer cohorts are February and June, respectively (Figure 3.4).

TRACE ELEMENT ANALYSIS

Age rather than mantle length data must be used to identify intra-annual squid cohorts and to estimate their growth rates because their growth rates show high plasticity and individuals of the same length can be from different seasonal cohorts (Arkhipkin *et al.,* 2020). As a result, the biological data analysis sections of TOR 3 focus on age analysis and identification of cohorts entering the U.S. *Illex illecebrosus* fishing grounds. The winter cohort was identified using statolith-based age analysis (Hendrickson 2004) as the primary cohort that supports the early part of the fishery period. However, the second cohort (now defined as the summer cohort, given the new information within this assessment), which supports the latter end of the fishery period, was inferred based on the average lifespan of the winter cohort (Hendrickson 2004).

In recent years, the use of trace elemental signatures as natural tags has been shown to have applications in determining population structure. Calcified structures including fish otoliths (Campana 1999), gastropod (Zacherl *et al.* 2003), jellyfish (Morrissey *et al.* 2020) and squid statoliths (Semmens *et al.* 2007, Avigliano *et al,* 2020) have been used to elucidate a variety of life history characteristics. Analogous to fish otoliths, statoliths are hard structures that grow continually throughout life and are formed by the deposition of calcium carbonate, principally in aragonite crystal form, within a protein matrix (Radtke 1983). As material is accumulated, trace elements are incorporated into the statolith microstructure (Arkhipkin 2005). Uptake of elements into the statolith microstructure is considered to reflect the environmental conditions at the time of incorporation, as well as reflecting physiological and genetic factors. They essentially act like a "black box" recording an individual's ecological history (Arkhipkin 2005). Statolith

microchemistry has proven to be an effective stock (Green *et al.* 2015, Avigliano *et al.* 2020) or cohort tag (Jones *et al.* 2018, Ching *et al.* 2019) in other species of squid, but trace element analysis has never been undertaken on *I. illecebrosus*.

This study aims to generate temporally resolved elemental chronologies of the 2020 statolith samples as a complimentary method to confirm the assignment of the winter and summer cohorts from the 2019 and 2020 age data.

Methods

Fishery samples were collected in 2020 as described above in the ageing methods section. A total of 551 individuals had their statoliths removed and stored in 96% ethanol. Of these, a subsample of 252 individuals were selected for trace element analysis to ensure that biweekly samples, both sexes and a range of maturities were represented (Table 3.4). These statoliths were mounted on microscope slides then ground and polished on one side to expose the nucleus following Arkhipkin and Shcherbich (2012).

Statoliths were analyzed for trace elements using laser ablation inductively coupled plasma mass spectrometry (LA-ICP-MS) at the Natural History Museum in London, UK. Statoliths were remounted onto shared slides of 30 to reduce the need to expose the ablation cell to external air sources, with contaminants removed from the ground surfaces using ethanol prior to analysis. Because the estimated elemental concentration can be substantially affected by instrumental drift, the analysis sequence was randomized so that the order of analysis for any one sample group was spread over the entire analysis sequence (Kerr and Campana 2014). Elemental concentrations were obtained using an ESI New Wave NWR193 laser ablation system coupled to an in-situ Agilent 7700 ICP-MS. Values for limit of detection (LOD) were calculated as 3 standard deviations (SD) of the background signal.

The following trace elements were quantified; Na, Sr, Mg, B, Li, Ba, Al, Mn, Fe, Zn, Cu, Cd and Pb, with Ca used as an internal standard to account for variation in ablation yield. A transect (25 μm in diameter) continuously acquired sample from the core (representing early ontogeny) to the edge of the dorsal dome (representing date of sample collection) at a rate of 3 μm s^{-1}, in the same direction as the ageing was undertaken (Figure 3.5).

The glass reference materials NIST-610 and NIST-612 (National Institute of Standards and Technology, USA) were used for external calibration. Both standards were ablated between every 5th statolith with NIST-610 used to calibrate elemental concentrations and assess changes in instrumental sensitivity and NIST-612 treated as an unknown sample to assess measurement accuracy.

Following trace element analysis, ablated statoliths were flipped and ground on the other side, embedded in mounting media (Canada Balsam™) and covered with a cover glass for observation (Arkhipkin and Shcherbich 2012). Statoliths were read under the transmitted light of an Olympus BX60 compound microscope at x400 magnification according to protocols outlined above in the Ageing section. Aged specimens were binned by month based on hatch date (hatch date = date of capture - mean of the last two age counts) and then assigned to a cohort based on the frequency

distribution of all sampled specimens, by hatch month, after expanding them to the total catch per trip. As previously discussed, squid hatched between November and April comprised the winter cohort and those hatched between May and July comprised the summer cohort.

All analyses were undertaken in R V.4.0.2 (R Core Team 2021). Elemental concentrations (ppm) were converted into molar concentrations (μmol.mol^{-1}, or mmol.mol^{-1} for Sr and Na given the high concentration of each element within the statolith microstructure) and standardized to calcium (element: Ca). Prior to analysis, data were post-processed to remove outliers given the noisy nature of the data. Values ±5 SD of the mean for each individual marker were considered outliers and removed from any subsequent analysis according to protocols described in Kerr and Campana (2014). As increments were counted every 25 μm using an eyepiece reticule during the ageing process, data were prepared for compatibility between datasets by binning the trace element data into 25 μm increments and calculating their average.

This analysis focuses on Sr:Ca, which is the most frequently analyzed element in hard biogenic structures. The data set consisted of multiple time observations for each statolith. Mixed modelling was therefore applied with Sr:Ca as the response variable, with the random intercept *slide number* (a unique identifier for each individual) used to model a dependency structure among Sr:Ca observations from the same squid. The random intercept was assumed to be normally distributed with mean 0 and variance σ^2. A Gaussian GAMM (identity link, to ensure positive fitted values) was used to determine whether Sr:Ca ratios were distinct for each assigned cohort and how they changed throughout ontogeny (Equation 1, below). Fixed categorical covariates available were *sex* (two levels), *cohort* (two levels), *location* (geographic location of sample collection, seven levels) and *maturity* (maturity stages 1-3 were coded as immature and stages 4-5 as mature for both sexes, two levels). Preliminary analysis indicated non-linear effects for hatch day and age. The variable *hatch* (day within the year, a continuous variable ranging from 1 to 365) had a smoother fitted using cyclic cubic regression splines, which are penalized cubic regression splines whose ends meet up to avoid discontinuity between December and January. The remaining fixed covariate, *age* (number of days post-hatching), is continuous and a smoother was fitted using thin plate regression splines, with one smoother fitted for each *cohort*.
Several models were fitted, with Akaike Information Criterion (AIC) used in conjunction with a backwards model selection procedure, to identify the optimal model according to the ten-step protocol described in Zuur *et al.* (2009) using "REML" estimation for the final model. Given that autocorrelation plots indicated violation of independence during model selection, an autocorrelation structure of order one (AR-1) was fitted for *age* nested within *slide number*, which significantly improved model fit and largely resolved autocorrelation issues. Model assumptions were verified by plotting standardized residuals against fitted values and against all potential covariates (Zuur and Ieno 2016). The optimal model was defined as:

$$Sr{:}\,Ca \sim f(age){:}\,cohort + f(hatch) + location + \ cohort \qquad (1)$$

where $f(age){:}\,cohort$ represents one smoother used for each *cohort* and *cohort* fitted as a mean term. All statistical modelling was performed using the R package "mgcv" (Wood 2017).

Results

The candidate models that explored the effects of biological variables on Sr:Ca ratios are given in Table 3.5. The beyond optimal model was fitted, and the optimal random structure was included to model dependency prior to the fixed components being optimized. Maturity was not significant at the 5% level for the beyond optimal model (MN1, Table 3.5) and was removed, which improved the AIC (MN2), but a log-likelihood test indicated that this did not significantly improve model fit ($\chi^2[1] = 3.42$, $p = 0.06$). Sex was not significant at the 5% level in MN2 and was also removed (MN3). This significantly improved model fit ($\chi^2[1] = 4.27$, $p = 0.04$), reduced degrees of freedom and lowered the AIC. Though the smoothers for the effect of age were significant for each *cohort*, *cohort* itself fitted as a mean term was marginally significant at the 5% level ($p = 0.03$) and therefore a model was run without the effect of *cohort* (MN4). This did not improve model fit.

Once the optimal fixed structure was identified (MN3), an autocorrelation plot of the standardized residuals was produced. This plot indicated substantial autocorrelation (Figure 3.6). Several different autocorrelation structures were fitted, but an AR-1 structure fitted for *age* nested within *slide number* provided the best model fit. A total of 5,651 Sr:Ca values were analyzed in the final optimal model (MN5) and model validation indicated no unresolved problems (Figure 3.7). Estimated regression parameters for the optimum model can be found in Table 3.6.

The most parsimonious model included the smoothing term *age* (representing the ontogenetic effect) modelled separately for the winter and summer cohorts. The F-values for both smoothers indicated a substantial effect of both cohorts on Sr:Ca concentration, and the summer cohort had lower expected degrees of freedom than the winter cohort, indicating a less complex trend, closer to linear (Table 3.6). A linear trend would have edf = 1, so substantial non-linear effects were evident for both cohorts. Fitted curves indicated substantial ontogenetic trends for both cohorts (Figure 3.8). Confidence intervals for the summer cohort were wider because the fishery is predominantly supported by the winter cohort and samples were obtained from commercial fishing vessels in-season, therefore a larger sample size of the winter cohort was available for analysis. Error increased in the model towards the latter stages of ontogeny, because those data are only represented by a few of the oldest individuals that have the longest trace element tracks.

Results

The ontogenetic trends revealed in this report for Sr:Ca ratios will be further investigated, along with the rest of the trace element concentrations measured in statoliths collected from the 2020 fishery samples, to elucidate migration patterns in *Illex illecebrosus.* However, this research is outside the scope of the current Terms of Reference for this assessment. For now, it is evident that ontogenetic trends are significantly different for each cohort and that removal of the cohort variable within the mixed model significantly impacts model fit. This finding provides additional support for partitioning of the cohorts based on hatch dates for both the 2019 and 2020 datasets.

Sr:Ca ratios have shown great potential to discriminate between population components in other species of squid. Only three species have been analyzed for cohort-specific trace element signals to date. Liu *et al.* (2015) analyzed the multivariate elemental signatures of another ommastrephid squid, *Dosidicus gigas*, and found no significant differences between the spring, fall and winter spawning cohorts. However, this was a preliminary analysis and sample size consisted of just 14 individuals, which substantially reduces the statistical power of the MANOVA applied to these

few samples. In addition, this was a solution-based study, which provides an integrated signal over the entire life history of an individual and does not account for ontogenetic changes. The loliginid squid, *Doryteuthis gahi*, has been found to have significantly different elemental signatures between the autumn and spring spawning cohorts within Falkland Islands waters. This has been confirmed using both solution-based (Arkhipkin *et al.* 2004) and laser-ablation-based methods (Jones *et al.* 2018). Cohort specific differences in Sr:Ca and Ba:Ca were also noted for another loliginid squid, *Sepioteuthis lessoniana* (Ching *et al*. 2019).

Differences in Sr:Ca ratios between cohorts has been attributed to the relationship between uptake of strontium into the statolith microstructure and temperature. Arkhipkin *et al.* (2004) found that Sr:Ca ratios among geographic locations were generally consistent with a negative correlation between Sr:Ca and temperature. A second study has shown that the ontogenetic profiles found within statoliths support the hypothesis of a negative correlation with temperature given what is already known regarding their patterns of migration (Jones *et al.* 2018). The only laboratory study undertaken on cephalopods to date failed to establish this relationship between temperature and strontium, but instead found a negative relationship between temperature and Ba:Ca (Zumholz *et al.* 2007). Sample size was also small in that study, with five individuals analyzed per treatment. However, that study was undertaken on cuttlefish which have very different life history traits (e.g., nektobenthic with much smaller ranges) than ommastrephid squids, the latter of which are nerito-oceanic and undergo extensive migrations during their lifespans. Because ommastrephid squid undergo extensive diel-vertical migrations that could mask patterns arising from horizontal migration, it has been suggested that it is more difficult to distinguish a clear strontium pattern in ommastrephid squid (Arkhipkin *et al*. 2004). However, our study indicates that this is not the case if the data are considered at high resolution and are temporally resolved.

In conclusion, the methodology used within our study is novel for ommastrephid squid, and has shown that the summer and winter cohorts have significantly different Sr:Ca ontogenetic signatures. Future analysis of the 2020 trace element data may help elucidate migration patterns to and from the fishing grounds, but for now presents further evidence that the winter and summer cohort assignments presented in this assessment are accurate.

Table 3.1. *Illex illecebrosus* sample sizes for dorsal mantle length (DML, mm), body weight (weight, g), sexual maturity and age (days), by month and sex, collected from the 2019 and 2020 catches of the directed fishery. The age samples are a subset of the DML, body weight and maturity samples. F and M represent females and males, respectively.

	Month	DML, body weight and maturity			Age		
Year	**Sampled**	**F**	**M**	**Total**	**F**	**M**	**Total**
2019	5	103	97	200	45	55	100
	6	141	60	201	67	32	99
	7			0			0
	8	113	140	253	50	52	102
	9	87	111	198	45	54	99
	10	44	55	99	0	0	0
	Total	**488**	**463**	**951**	**207**	**193**	**400**
2020	5			0			0
	6	62	80	142	14	26	40
	7	320	377	697	60	72	132
	8	139	182	321	52	57	109
	9			0			0
	10	53	56	109	25	19	44
	Total	**574**	**695**	**1,269**	**151**	**174**	**325**

Table 3.2. Summary of samples sizes and means of dorsal mantle length (DML, mm), body weight (g) and age (days) and their standard errors (SE) for the winter cohort (individuals hatched during November-April) of *Illex illecebrosus*, by sex and catch month, during 2019 and 2020.

Year	Sex	Catch month	N	DML (mm)	SE	Body Weight (g)	SE	N Ages	Age (days)	SE
2019	**F**	May	103	196.4	2.5	143.3	5.5	45	164.2	2.9
		June	141	219.3	1.3	200.7	3.8	67	153.7	1.5
		July	0					0		
		Aug	113	210.1	2.8	198.1	9.5	49	147.2	3.1
		Sept	81	234.3	1.9	266.4	6.7	39	177.9	2.3
		Oct	44	235.0	3.9	268.2	12.0	0		
		Total N	**482**					**200**		
	M	May	97	181.7	2.0	117.8	3.6	55	160.7	2.5
		June	60	203.4	1.5	166.4	5.0	32	147.9	2.8
		July	0					0		
		Aug	139	189.1	1.7	151.4	5.5	52	146.1	3.2
		Sept	107	212.8	1.2	236.6	5.0	50	174.8	1.7
		Oct	55	213.8	2.4	223.9	7.6	0		
		Total N	**458**					**189**		
2020	**F**	May	0					0		
		June	62	165.8	1.1	94.5	2.1	14	147.9	2.2
		July	320	186.3	0.9	136.6	2.2	60	164.8	1.9
		Aug	139	208.0	1.5	165.3	4.5	52	174.4	1.9
		Sept	0					0		
		Oct	30	116.0	4.3	34.0	3.2	2	169.5	5.5
		Total N	**551**					**128**		
	M	May	0					0		
		June	80	163.5	1.1	94.9	2.0	26	150.5	2.0
		July	377	179.9	0.8	128.5	1.8	72	166.1	1.4
		Aug	182	195.9	0.8	141.4	1.9	57	168.6	1.5
		Sept	0					0		
		Oct	38	125.9	3.9	43.8	3.3	1	-	-
		Total N	**677**					**156**		

Table 3.3 Summary of samples sizes and means of dorsal mantle length (DML, mm), body weight (g) and age (days) and their standard errors (SE) for the summer cohort (individuals hatched during May-July) of *Illex illecebrosus*, by sex and catch month, during 2020.

Year	Sex	Catch month	N	DML (mm)	SE	Body Weight (g)	SE		Age (days)	SE
2020	**F**	Oct	23	114.7	5.4	32.8	3.8	23	103.8	3.5
	M	Oct	18	129.9	4.6	44.7	3.7	18	115.8	4.3

Table 3.4. Means and standard errors (SE) of dorsal mantle length (DML, mm) and age (days), by sex and month sampled, of the aged *Illex illecebrosus* samples, from the 2020 directed fishery, included in the trace element analysis.

Sex	Month Sampled	N	DML (mm ±SE)	Age (days ±SE)
F	June	14	163.9 ± 1.3	147.9 ± 2.2
	July	53	193.6 ± 2.4	164.3 ± 2.1
	August	24	213.8 ± 4.6	178.0 ± 3.8
	October	25	117.6 ± 5.3	109.0 ± 4.9
	Total sample size F	**116**		
M	June	26	163.1 ± 1.5	150.5 ± 2.0
	July	55	183.9 ± 2.0	164.6 ± 1.6
	August	36	194.8 ± 1.7	168.9 ± 2.1
	October	19	130.6 ± 4.5	118.5 ± 4.7
	Total sample size M	**136**		

Table 3.5. Models applied to the Sr:Ca concentrations of *Illex illecebrosus* statoliths, numbered for reference (MN) within the text, with all models containing the random intercept slide number to model dependency. The notation f(age): $cohort$ means that one smoother was used for each cohort and *cohort* was fitted as a mean term and $\varepsilon_i \sim N(0,\sigma^2)$. df = degrees of freedom, %DE = percentage deviance explained, AIC = Akaike's Information Criterion. The model with the best fit is shown in bold-faced text.

MN	Model	df	%DE	AIC
1	Sr:Ca ~ f(age):cohort + f(hatch) + location + sex + maturity	17	27.6	5780
2	Sr:Ca ~ f(age):cohort + f(hatch) + location + sex	16	27.6	5775
3	Sr:Ca ~ f(age):cohort + f(hatch) + location	15	27.5	5768
4	Sr:Ca ~ f(age) + f(hatch) + location	12	25.3	5847
5	**Sr:Ca ~ f(age):cohort + f(hatch) + location + AR-1 structure**	**16**	**21.4**	**727**

Table 3.6. Estimated regression parameters for the generalized additive mixed model for the response variable Sr:Ca as presented in Equation 1. Expected degrees for freedom (edf) for smooth terms included, significant p-values indicated by *.

Explanatory Variable	edf	F-value	p-value
cohort	-	0.43	0.51
location	-	5.39	<0.001 *
age: winter cohort	8.50	62.44	<0.001 *
age: summer cohort	6.17	27.70	<0.001 *
hatch	3.98	4.13	<0.001 *

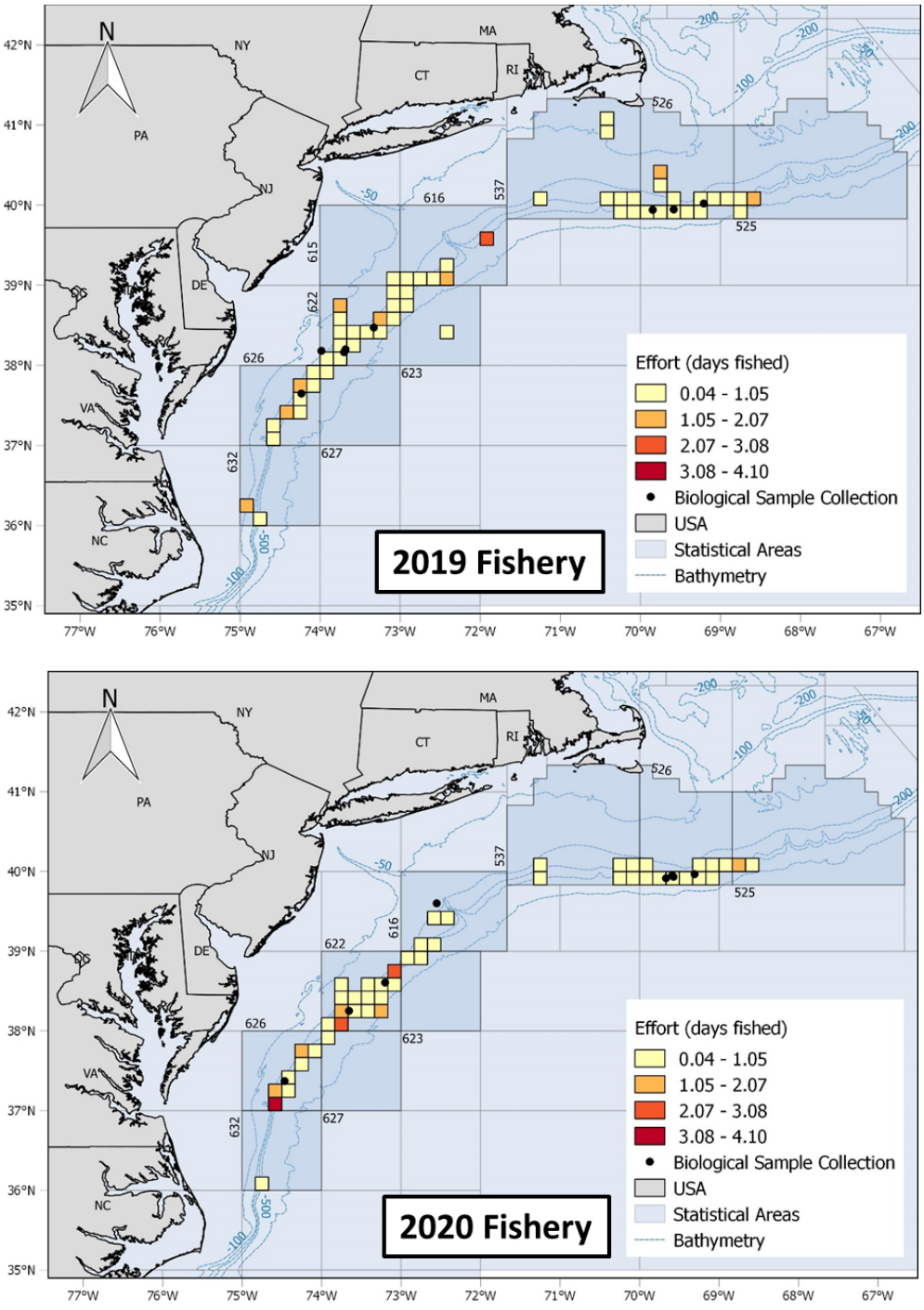

Figure 3.1. *Illex illecebrosus* biological sampling locations (black dots) overlain on fishing effort (days fished), by ten-minute square (TNMS), for the directed fishery during 2019 and 2020. During each year, one sampling location is located outside of a TNMS because several TNMSs were deleted from each map due to inaccurate fishing location reporting on some Vessel Trip Reports The deleted TNMSs were located either too far inshore or offshore from the known fishing grounds along the edge of the continental shelf. Isobaths are shown in meters.

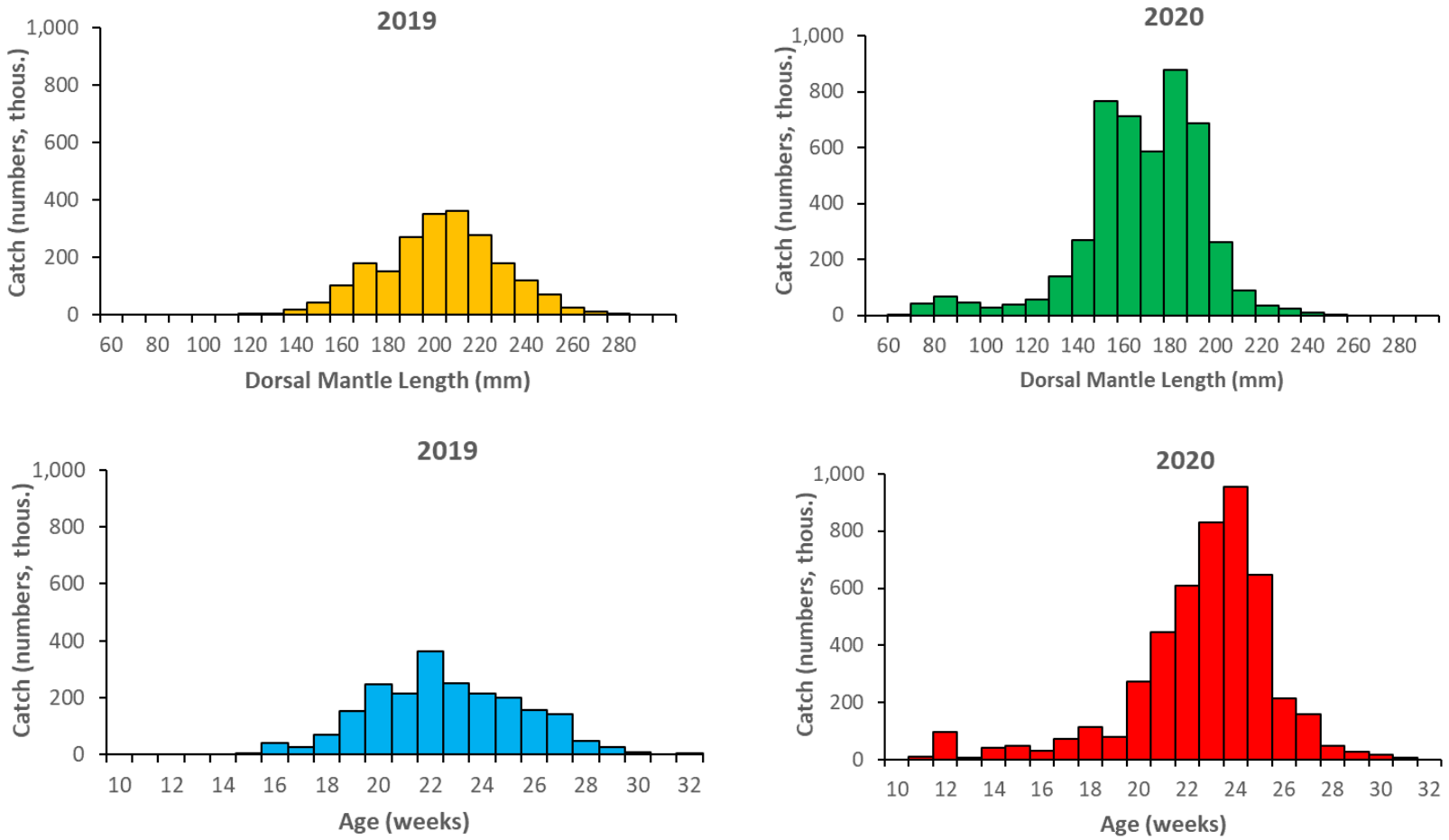

Figure 3.2. Length compositions (mm) and age compositions (days binned by week) of the *Illex illecebrosus* catches in the 2019 and 2020 *I. illecebrosus* fisheries.

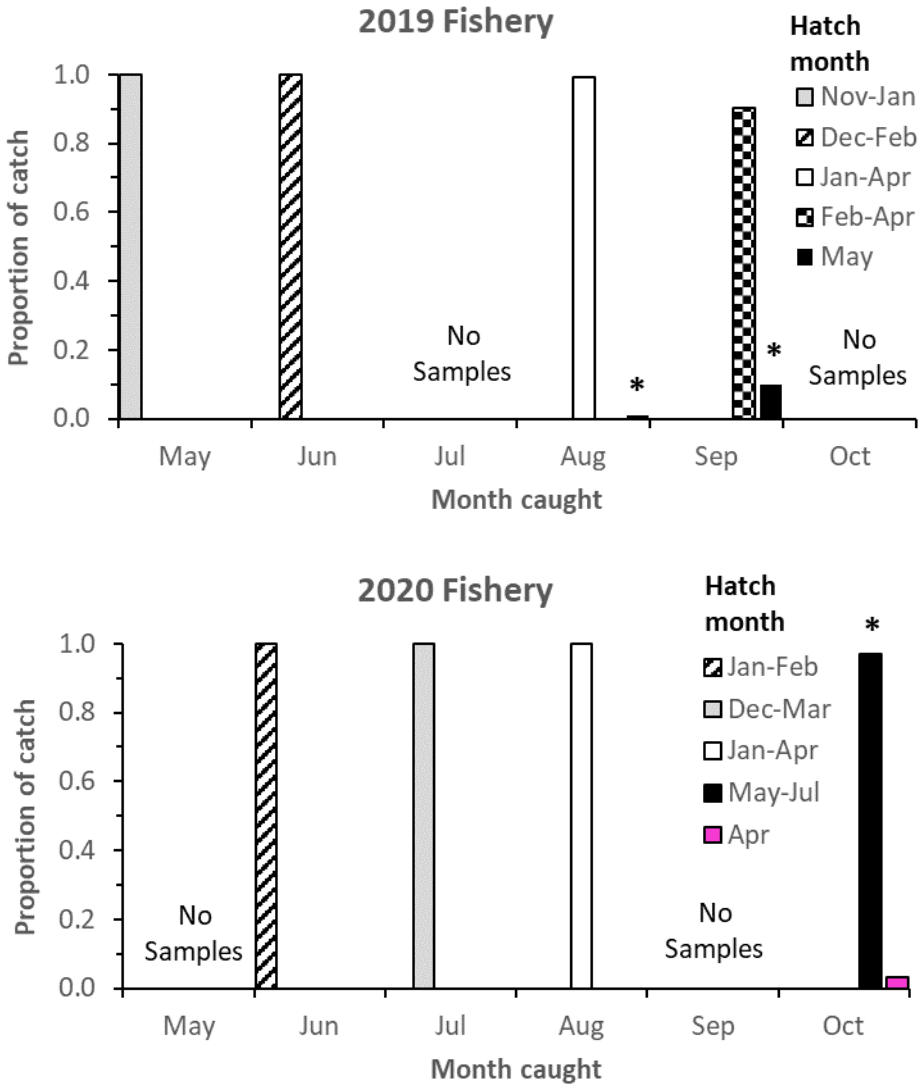

Figure 3.3. Hatch month compositions of *Illex illecebrosus*, as the proportions of monthly catch, in the 2019 and 2020 *I. illecebrosus* fisheries. The winter cohort is comprised of individuals hatched during November-April and the summer cohort is comprised of individuals hatched during May-July (denoted by asterisks).

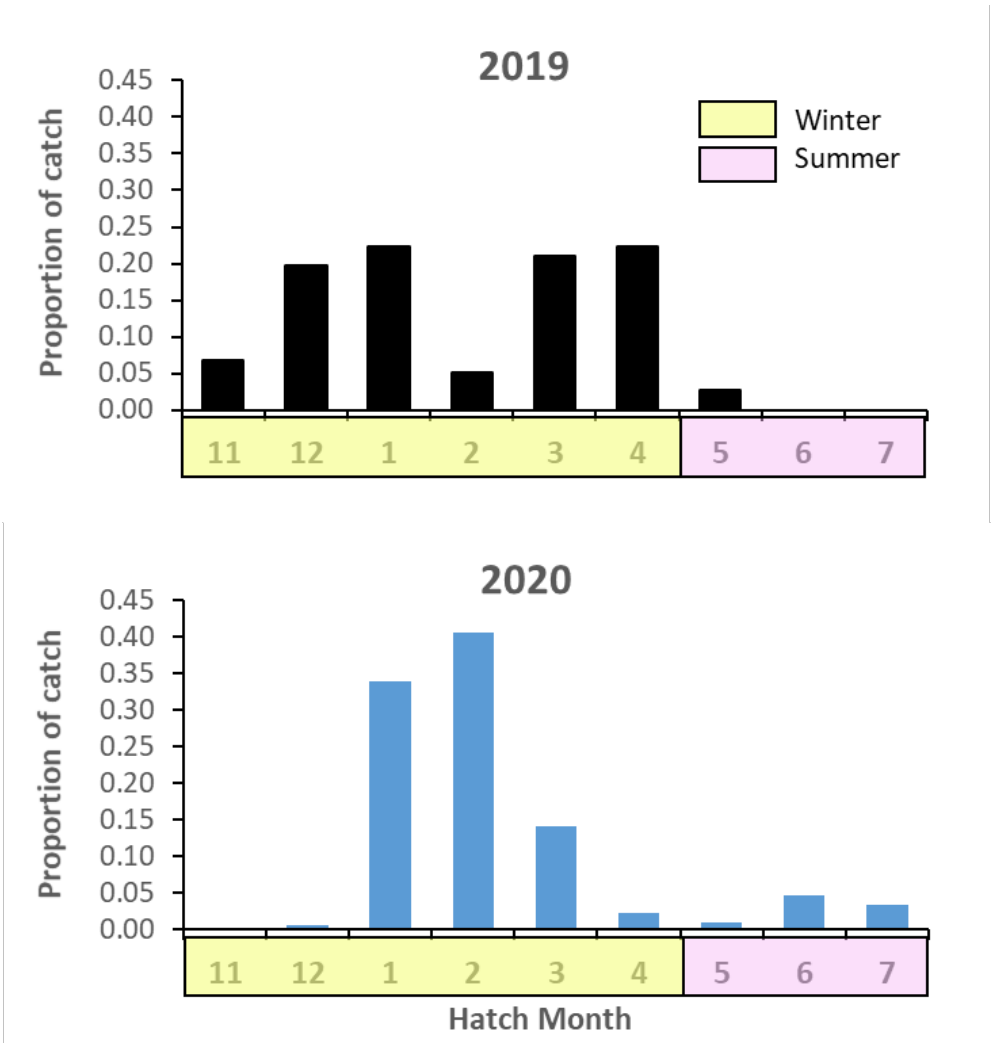

Figure 3.4. *Illex illecebrosus* intra-annual cohorts (winter and summer), identified from age frequency data (shown as proportions of the 2019 and 2020 catches) by hatch month, that support the U.S. *I. illecebrosus* fishery. Ages were estimated from counts of statolith daily growth increments. Catch proportions differ by hatch month between years because of differential sampling; May-June and August-September (no July or October samples) during 2019 and June-August and October (no May or September samples) during 2020. For example, the low proportions of individuals hatched in February and June and July during 2019 were due to the lack of samples during July and October, respectively. Due to these temporal sampling difference, the two years must be viewed collectively to identify the modal hatch months of each cohort; February and June for the winter and summer cohorts, respectively.

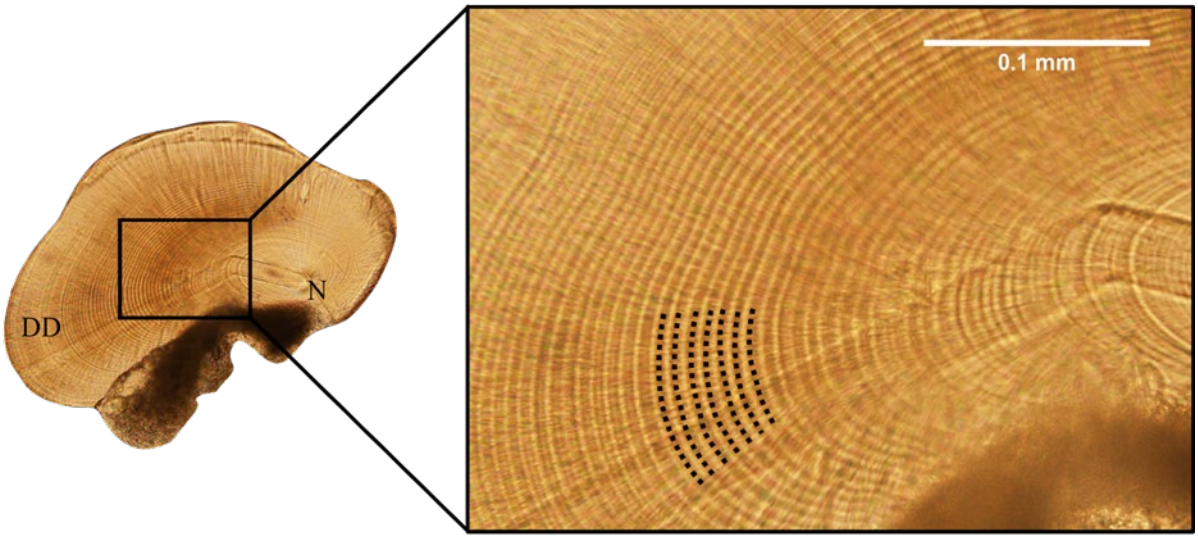

Figure 3.5. Image of a ground statolith with a trace element ablated transect extending from the nucleus to the edge of the dorsal dome. Dotted lines in the insert indicate seven growth increments, N = nucleus, DD = dorsal dome.

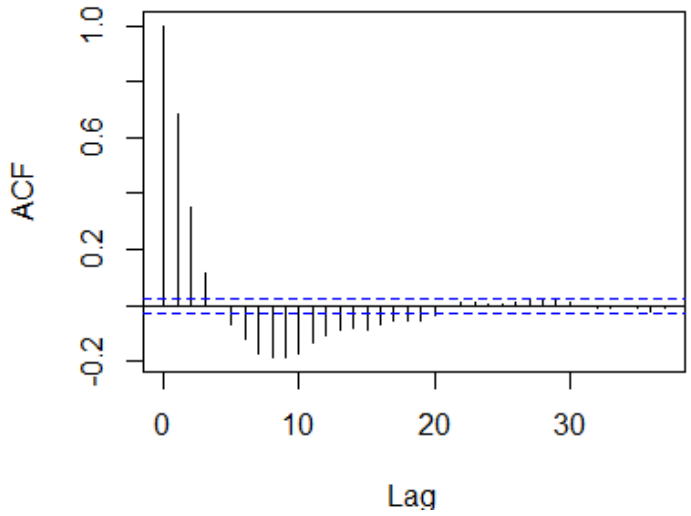

Figure 3.6. Autocorrelation plot of the standardized residuals from model MN5 (refer to Table 3.5).

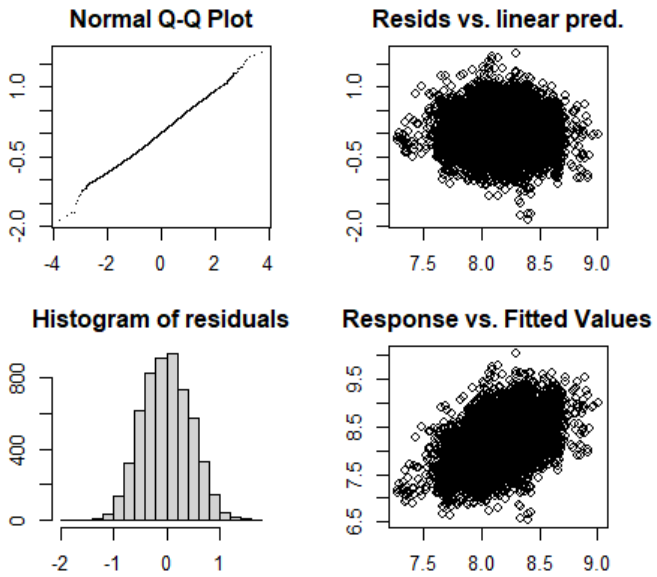

Figure 3.7. Residuals from optimal model (MN5) for Sr:Ca ratios, as defined in Equation 1.

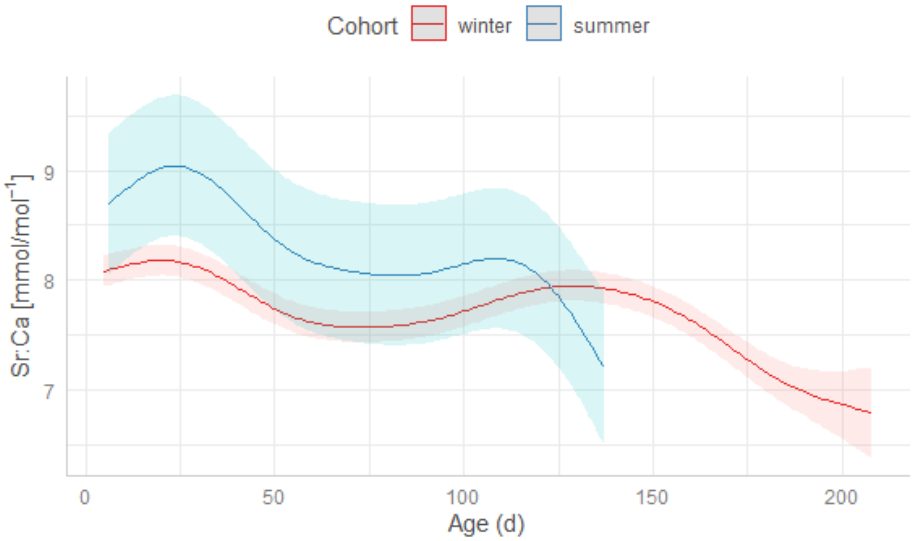

Figure 3.8. Fitted curves based on model predictions for the concentration of Sr:Ca ratios in relation to post-hatching age in days, with individual smoothing curves for each cohort and 95% confidence intervals (shaded).